Optical mesh lattices with $\mathcal{PT}$ symmetry

Mohammad-Ali Miri,[1,*] Alois Regensburger,[2,3] Ulf Peschel,[2] and Demetrios N. Christodoulides[1]
[1]*CREOL/College of Optics, University of Central Florida, Orlando, Florida 32816, USA*
[2]*Institute of Optics, Information and Photonics, University of Erlangen-Nuernberg, 91058 Erlangen, Germany*
[3]*Max Planck Institute for the Science of Light, 91058 Erlangen, Germany*
(Received 7 June 2012; published 3 August 2012)

We investigate a class of optical mesh periodic structures that are discretized in both the transverse and longitudinal directions. These networks are composed of waveguide arrays that are discretely coupled, while phase elements are also inserted to discretely control their effective potentials and can be realized both in the temporal and the spatial domain. Their band structure and impulse response are studied in both the passive and parity-time ($\mathcal{PT}$)-symmetric regime. The possibility of band merging and the emergence of exceptional points, along with the associated optical dynamics, are considered in detail both above and below the $\mathcal{PT}$-symmetry breaking point. Finally, unidirectional invisibility in $\mathcal{PT}$-synthetic mesh lattices is also examined, along with possible superluminal light transport dynamics.

DOI: 10.1103/PhysRevA.86.023807 PACS number(s): 42.25.Bs, 11.30.Er, 42.82.Et

I. INTRODUCTION

Optical wave propagation in periodic structures has been a theme of considerable attention in the last 20 years or so [1–5]. In general, such arrangements can exhibit intriguing and potentially useful light dynamics that are otherwise impossible in the bulk. Periodic Bragg gratings and two- and three-dimensional photonic crystals with a complete band gap are examples of such configurations. Optical waveguide arrays represent yet another class of periodic structures and have been the focus of intense research in the last decade [6–14]. As indicated in several studies, optical arrays can be used as versatile platforms to observe a number of processes, ranging from Bloch oscillations [9,10] to Landau-Zener tunneling [11], and from Anderson localization [12] to discrete solitons [6,7], Rabi oscillations [13], and dynamic localization [14], just to mention a few. Along similar lines, longitudinally periodically modulated optical waveguide arrays have also been studied in several works [15,16].

Quite recently, the concept of parity-time ($\mathcal{PT}$) symmetry has been introduced in the field of optics [17–19]. Interestingly, the very idea of $\mathcal{PT}$ symmetry originated within the framework of quantum mechanics through which a large class of complex non-Hermitian Hamiltonians was identified that could, in principle, exhibit entirely real spectra [20,21]. This can happen as long as the associated Hamiltonian and the combined $\mathcal{PT}$ operator share the same set of eigenfunctions. In this case, this is possible provided that the corresponding complex potential satisfies the condition $V^*(x) = V(-x)$ [20]. This directly implies that the real and imaginary parts of the potential must be even and odd functions of position, respectively.

Lately, optical $\mathcal{PT}$ symmetry has been experimentally observed in two-element coupled systems where nonreciprocal dynamics (disrupting left-right symmetry) and spontaneous $\mathcal{PT}$-symmetry breaking have been demonstrated [22,23]. What made this transition to photonics possible is the isomorphism between the evolution equations in quantum mechanics and optics. Indeed, one can show that the complex refractive index, $n(x) = n_R(x) + in_I(x)$, plays in this case the role of an optical potential. In this representation, the real part $n_R(x)$ stands for the refractive index profile, while the imaginary part $n_I(x)$ represents the gain or loss in the system (depending on its sign). Clearly, under $\mathcal{PT}$-symmetric conditions, one expects that $n_R(x) = n_R(-x)$ and $n_I(x) = -n_I(-x)$. In other words, the index distribution must be an even function of position, whereas the gain and loss must be antisymmetric. Thus far, several works have pointed out that $\mathcal{PT}$ symmetry can lead to altogether new optical dynamics, which are otherwise impossible in standard passive optical arrangements [24–41]. These may include, for example, the occurrence of abrupt phase transitions, along with the appearance of the so-called exceptional points [24–26], power oscillations [18], breaking left-right symmetry, and the occurrence of secondary emissions [18]. In addition, new classes of optical solitons [19,38] and nonlinear $\mathcal{PT}$ optical isolators [29] have been suggested, along with unidirectional invisibility [35,36], broad-area $\mathcal{PT}$ single-mode lasers [30], and coherent perfect absorbers [32–34]. Note that phase transitions similar to those occurring due to $\mathcal{PT}$-symmetry breaking have also been reported in other systems involving gain and loss modulation [42].

So far, however, experimental observations of $\mathcal{PT}$ symmetry in optics have been carried out in basic coupled systems involving only two elements [22,23]. What has hindered progress along these lines is not only the delicate balance needed between gain and loss, but also the requirement that the real part of the potential should remain symmetric, even in the presence of gain and loss. Fulfilling all of these conditions at the same time is by itself a challenging task because of the underlying Kramers-Kronig relations. Therefore, of interest would be to develop a new class of optical platforms where refractive effects and gain or loss can be treated separately and thus facilitate the realization of $\mathcal{PT}$-symmetric optics on a large scale. This goal is reached by discretizing not only the transverse but also the longitudinal or propagation direction.

In this work, we introduce a class of $\mathcal{PT}$-symmetric optical lattices. These mesh arrangements are composed of an array of waveguides with each one being discretely and periodically coupled to its adjacent neighbors [Fig. 1(a)]. Unlike ordinary waveguide arrays, light propagation in such mesh systems is

*miri@knights.ucf.edu

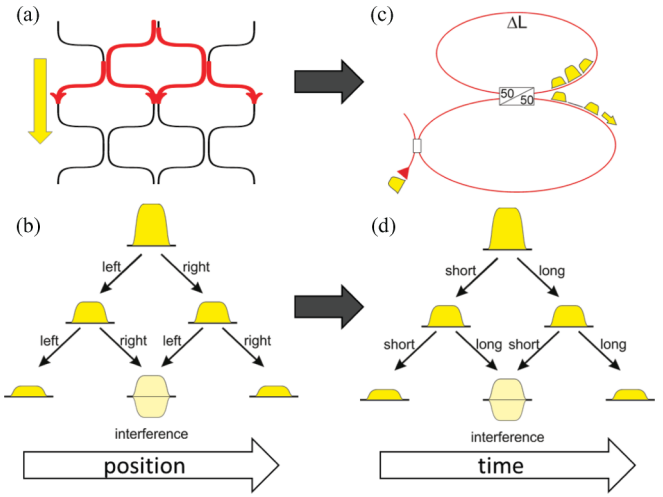

FIG. 1. (Color online) (a) Discrete mesh lattice in the spatial domain; (b) pulses in the spatial lattice propagate to the left and right on a discrete 1D position grid; (c) equivalent time-multiplexed scheme involving two coupled fiber loops with a length difference ΔL; and (d) pulses in the short (long) loop are advanced (delayed) in time, thus making discrete steps on a 1D temporal grid. The propagation dynamics are identical to those expected in (b).

discretized in two dimensions (transverse and longitudinal). The band structure of this family of mesh lattices is derived analytically and its effects on light dynamics are investigated. Because of the aforementioned two-dimensional (2D) discretization, the resulting band structure is characterized by both a transverse and a longitudinal Bloch momentum.

As we will see, this type of lattice can provide a versatile platform for observing a host of $\mathcal{PT}$-symmetric phenomena and processes. Along these lines, phase elements can be readily inserted in the mesh lattice so as to control the real part of the array potential, while amplifiers (that are turned on or off) can be included to provide the needed antisymmetric gain-loss profile. The fundamental building block of such a mesh structure happens to be a basic $\mathcal{PT}$-symmetric coupler arrangement. What makes this structure practically appealing is the physical separation between the coupling and amplification or attenuation stages within this building block. Band-merging effects as well as the emergence of exceptional points are investigated in this family of $\mathcal{PT}$ lattices, along with superluminal light transport. Finally, unidirectional invisibility in $\mathcal{PT}$-synthetic mesh lattices is also examined and pertinent examples are provided.

II. OPTICAL MESH LATTICES IN THE TIME DOMAIN

Lately, the temporal equivalent of an optical mesh lattice has been experimentally realized using time-multiplexed loop arrangements [43]. Such configurations have been systematically employed to investigate a number of issues, ranging from discrete quantum walks [44–47] to Bloch oscillations and fractal patterns [43,48]. While spatial realizations of such mesh lattices have also been reported [47,49], time-multiplexed fiber loop schemes have so far demonstrated a high degree of flexibility [43,45]. In time-multiplexed schemes, a discrete time axis n corresponds to the transverse discrete axis of a corresponding spatial optical mesh lattice, as shown in Figs. 1(c) and 1(d). These time-multiplexed configurations involve two coupled fiber loops that are coupled via a central 50:50 directional coupler. These two fiber loops differ in length by ΔL. Here, the equivalent transverse coupling to the left and right sites is enabled by this length difference between the two loops. An independent discretization in time is then obtained by monitoring the round-trip number m in these loops. Hence, the system is essentially discretized in two dimensions. As we will see, the propagation dynamics of light pulses in such discrete temporal lattices is exactly identical to those expected in the spatial configurations discussed in Sec. III of this paper.

In an experimental setup, gain and loss can be readily integrated into the fiber loops, e.g., by standard semiconductor or fiber-optical amplifiers and amplitude modulators. This in turn may enable the demonstration of large-scale $\mathcal{PT}$-synthetic optical lattices in the temporal domain [50]. Given that the "topological" arrangements of a temporal and a spatial mesh lattice are totally equivalent, here, without any loss of generality, we will consider for simplicity their spatial realization.

III. OPTICAL MESH LATTICE AND ITS BAND STRUCTURE

Figure 2 illustrates the spatial realization of such a mesh lattice when only passive phase elements are involved. As previously indicated, this configuration can be synthesized using an array of waveguides that are periodically and

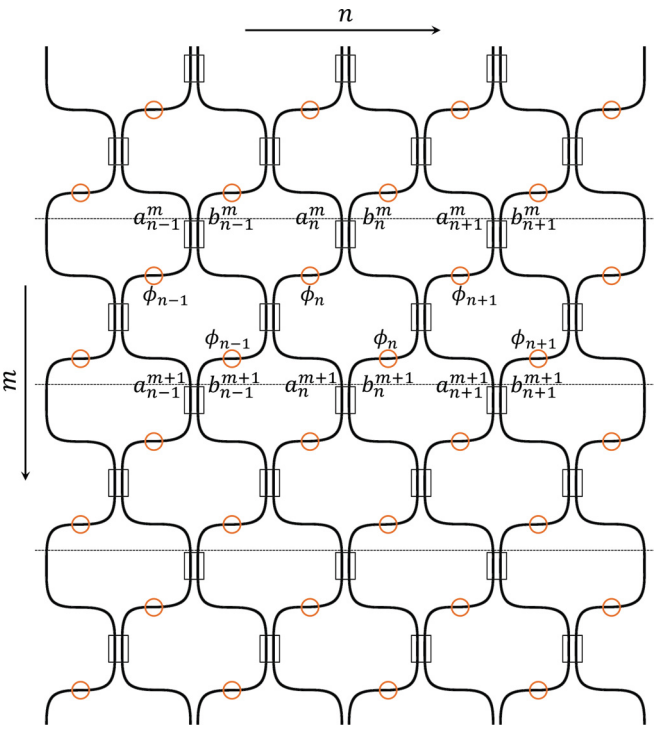

FIG. 2. (Color online) An optical mesh lattice. The lattice is composed of an array of waveguides, which are periodically coupled together in discrete intervals. Circles indicate the position of phase elements and rectangles indicate the coupling regions. The dashed lines show the discrete points where the field intensity is evaluated before coupling occurs.

discretely coupled to their next neighbors (at the rectangular regions of Fig. 2). In addition, phase elements can also be inserted. Each phase element introduces at every array site n a phase ϕ_n that happens to be independent of the discrete propagation step m. The location of each phase modulator in the lattice is denoted in the figure by a circle. As we will later demonstrate, these phase modulators effectively play the role of a refractive index profile in continuous arrangements. Figure 1(a) schematically shows how light flows in such a system when only one of the waveguides is initially excited. After traveling a certain distance in each waveguide, light couples to the adjacent left (right) channel through a coupler, and after propagating this same distance it then couples to the adjacent waveguide to its right (left). Indeed, light propagation in this system leads to an interference process that is equivalent to a discrete time quantum walk [44,51,52].

As Fig. 2 clearly indicates, this mesh lattice is diatomic in nature. Using the simple input-output relation of a 50:50 coupler [53] and by considering the effect of the phase elements, it is straightforward to show that the light evolution equation in this system takes the form

$$a_n^{m+1} = \frac{e^{i\phi_n}}{2}\left[\left(a_n^m + ib_n^m\right) + e^{-i\phi_n}\left(-a_{n-1}^m + ib_{n-1}^m\right)\right], \quad (1a)$$

$$b_n^{m+1} = \frac{e^{i\phi_n}}{2}\left[\left(b_n^m + ia_n^m\right) + e^{i\phi_{n+1}}\left(-b_{n+1}^m + ia_{n+1}^m\right)\right]. \quad (1b)$$

In Eqs. (1), a_n^m and b_n^m represent the field amplitudes at adjacent waveguide sites n (in the nth column) at a discrete propagation step or distance m (mth row). It should be noted that in deriving these equations, the phase accumulated due to propagation in any waveguide section is ignored. Indeed, a waveguide section of length l between two subsequent couplers leads to a phase accumulation of βl, where β is the propagation constant of the guide. Yet, one can readily show that even in the presence of these additional phase terms, Eqs. (1) remain the same once a simple gauge transformation is used, $(a_n^m, b_n^m) \rightarrow (a_n^m, b_n^m)e^{i2m\beta l}$.

To establish the necessary periodicity, we assume that the phase elements provide a phase potential that alternates between two different values in n:

$$\phi_n = \begin{cases} +\phi_0, & n = \text{even}, \\ -\phi_0, & n = \text{odd}. \end{cases} \quad (2)$$

This kind of phase potential has a translational symmetry, $\phi_{n+2} = \phi_n$, which leads to a transverse periodicity in this "four-atom" lattice with a fundamental period of $N = 2$ where each cell is diatomic. In addition, the lattice is now periodic in both n and m.

First we study the band structure of this mesh system. Once the band characteristics and corresponding Bloch modes are known, the dynamic properties of the system can then be extrapolated. To find the dispersion relation of this lattice, we consider discrete "plane-wave solutions" of the form $e^{iQn}e^{i\theta m}$, where Q represents a Bloch momentum in the transverse direction and θ plays the role of a propagation constant. To obtain the corresponding band structure, we assume solutions

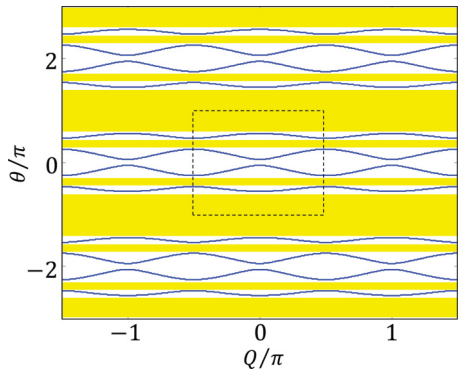

FIG. 3. (Color online) Band structure of the optical mesh lattice in the presence of a periodic steplike potential created from phases, alternating between $-\phi_0$ and $+\phi_0$, where $\phi_0 = 0.2\pi$. The shaded area shows the band-gap regions and the dotted boundary depicts the primary Brillouin zone of this lattice.

of the form

$$\begin{pmatrix} a_n^m \\ b_n^m \end{pmatrix} = \begin{pmatrix} A_n \\ B_n \end{pmatrix} e^{iQn}e^{i\theta m}, \quad (3)$$

where A_n and B_n are periodic Bloch functions with the period of $N = 2$, i.e., $A_{n+2} = A_n$ and $B_{n+2} = B_n$. In general, for $n = 2j$, we use $A_n, B_n = A_0, B_0$, while for $n = 2j + 1$, we employ $A_n, B_n = A_1, B_1$. This comes from the fact that a unit cell of this periodic structure includes two discrete positions n.

By inserting Eqs. (3) in (1), and by adopting the phase potential of Eq. (2), we obtain the following dispersion relation after expanding the corresponding 4×4 determinant of a unit cell:

$$\cos(2Q) = 8\cos^2(\theta) - 8\cos(\phi_0)\cos(\theta) + 4\cos^2(\phi_0) - 3. \quad (4)$$

As expected from the double periodicity of this system in both n and m, the band structure is also periodic in both Q and θ, having fundamental periods of π and 2π, respectively. This represents a major departure from optical waveguide arrays where the propagation dimension is a continuous variable. Under the assumption of Eq. (2), this mesh arrangement exhibits four primary bands, which are periodic with respect to the two Bloch momenta. Figure 3 depicts the band structure of this mesh lattice when $\phi_0 = 0.2\pi$.

Equation (4) is valid, in general, for any arbitrary choice of ϕ_0. However, it should be noted that in the special case where $\phi_0 = 0$ (empty lattice), this relation becomes degenerate. Indeed, for the empty lattice, the periodicity of this diatomic lattice is $N = 1$ and hence its Brillouin zone involves two bands and lies in the domain of $-\pi < Q < \pi$ and $-\pi < \theta < \pi$. The folded version of this Brillouin zone (corresponding to the empty lattice) is shown in Fig. 4(a), where the two bands are degenerately folded into four. Figures 4(b)–4(d) depict the band structure of this mesh lattice for three nonzero values of ϕ_0 within the Brillouin zone as a function of the Bloch momenta, i.e., $-\pi/2 < Q < \pi/2$ and $-\pi < \theta < \pi$. Again, the shaded areas show the associated band gaps. According to Fig. 4, a nonzero ϕ_0 lifts the degeneracy and leads, indeed, to four bands.

According to Eq. (4) and as one can see from the figures, the band structure has a reflection symmetry around $Q = 0$ and

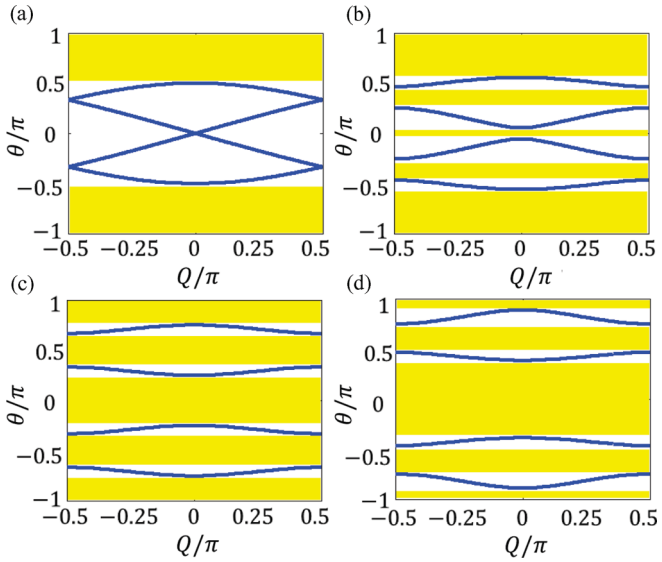

FIG. 4. (Color online) Band structure of an optical mesh lattice for several cases: (a) Lattice without any phase potential $\phi_0 = 0$ (empty lattice), (b) Lattice with a symmetric phase steplike potential varying between $-\phi_0$ and $+\phi_0$ when $\phi_0 = 0.2\pi$, (c) Same as in (b), but with $\phi_0 = 0.5\pi$, and (d) $\phi_0 = 0.7\pi$. For (a), the reduced Brillouin zone is depicted, while for the rest, the first Brillouin zone is shown in its entirety.

$\theta = 0$. For any finite ϕ_0, there are four bands in the Brillouin zone, all having a zero slope at the center ($Q = 0$) and at the edges ($Q = \pm\pi/2$). For the empty lattice, on the other hand, in reality there are two bands and the slope is zero at the center ($Q = 0$) of the top band, while it is nonzero at the two edges ($Q = \pm\pi/2$) and at $Q = \theta = 0$, where the bands collide and there is no band gap between them. The addition of the phase potential $\pm\phi_0$ to the empty lattice breaks this degeneracy and creates band gaps at these points. This breaking of the degeneracy becomes clear by comparing Figs. 4(a) and 4(b). Equation (4) can also be written in a more explicit form as a function of Q:

$$\theta = \pm\cos^{-1}\left\{\tfrac{1}{2}[\cos(\phi_0) \pm \sqrt{\cos^2(Q) + \sin^2(\phi_0)}]\right\}, \qquad (5)$$

where in this relation any combination of the two plus and minus signs corresponds to each of the four bands.

Before ending this discussion, it is worth noting that this phase potential does not need to be symmetrized in a $\pm\phi_0$ fashion, as done above. In fact, any periodic potential that is alternating in n between two different phase values will break the degeneracy of an empty lattice, thus creating four bands in the first Brillouin zone. For example, let us consider a phase potential that varies between 0 and $2\phi_0$ in n:

$$\phi_n = \begin{cases} 2\phi_0, & n = \text{even}, \\ 0, & n = \text{odd}. \end{cases} \qquad (6)$$

Note that this latter phase potential has the same strength as the one used before. In this latter case, by using the same ansatz of Eq. (3), we directly obtain the dispersion relation corresponding to the new potential of Eq. (6):

$$\cos[2(Q + \phi_0)] = 8\cos^2(\theta - \phi_0) - 8\cos(\phi_0)\cos(\theta - \phi_0) + 4\cos^2(\phi_0) - 3. \qquad (7)$$

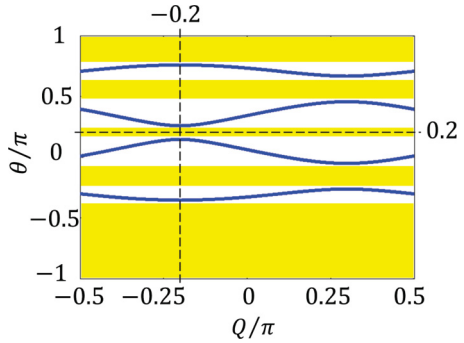

FIG. 5. (Color online) Band structure of an optical mesh lattice with a nonsymmetric steplike phase potential alternating between 0 and $2\phi_0$, while $\phi_0 = 0.2\pi$. Compared to the case of a symmetric phase potential [Fig. 4(b)], the band structure is shifted from the center.

A close examination of Eq. (7) reveals that this latter dispersion curve is identical to that of Eq. (4), apart from a phase shift in both θ and Q. More specifically, Q has shifted by an amount of $-\phi_0$, while θ has shifted by ϕ_0. Figure 5 shows a plot of this dispersion relation for $\phi_0 = 0.2\pi$. The shift of origin compared to Fig. 4(b) is evident in this figure.

In the rest of this work, we consider, for simplicity, symmetric phase potentials for which the band structure is symmetric around $Q = \theta = 0$.

IV. OPTICAL DYNAMICS IN MESH LATTICES

In this section, we investigate optical dynamics in passive mesh lattices. The impulse response of the system is of particular importance, since it is known to excite the entire band structure. For this reason only, one of the waveguide elements is excited at $m = 0$. In what follows, the impulse response will be studied by using $a_0^0 = 1$, with all the other elements in the array initially set to zero.

Figure 6(a) shows the impulse response of this array lattice when $\phi_0 = 0$. According to this figure, light transport in this system exhibits upon spreading a highest slope of $\Omega_{\max} = \pm 1/\sqrt{2}$ with respect to the longitudinal axis. As we will see, this result will be formally justified by considering the group velocity in this arrangement. The impulse response of the mesh lattice in the presence of a periodic phase potential with $\phi_0 = 0.4\pi$ is also plotted in Fig. 6(b). In this last case, it becomes apparent that the maximum speed of the excitation spreading becomes slower when ϕ_0 increases. As in waveguide arrays [6], the impulse response can be viewed as a "ballistic" transport across the array.

The band structure can also provide useful information concerning the evolution of more complicated initial excitations such as localized wave packets. More specifically, we consider initial distributions of a_n^0 and b_n^0 of the form $f_n e^{iQ_0 n}$, where f_n is a slowly varying envelope function (with a narrow spatial spectrum) and $e^{iQ_0 n}$ is a rapidly varying phase term signifying the central Bloch momentum Q_0 of this wave packet. Therefore, the propagation process of this discrete beam excitation can be effectively treated through a Fourier superposition of the Floquet-Bloch modes $e^{iQn}e^{i\theta m}$ assumed before to analyze this system. In this regard, both the group velocity and the dispersion broadening of this wave packet

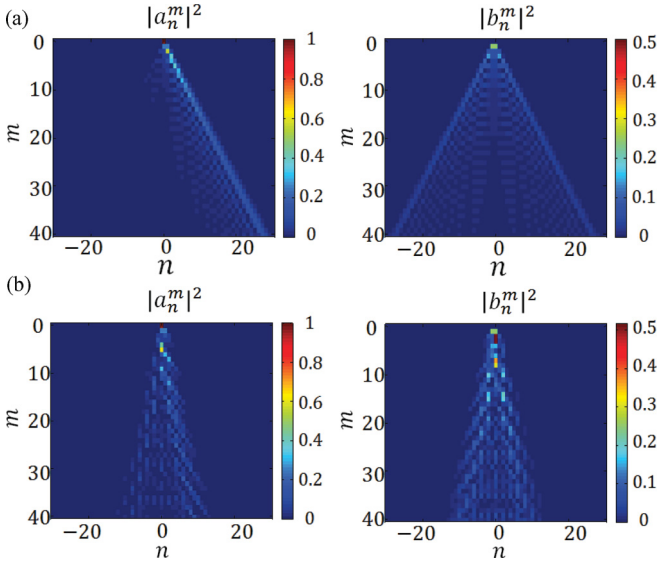

FIG. 6. (Color online) Impulse response of a mesh lattice where the intensity profile of a_n^m and b_n^m is plotted: (a) $\phi_0 = 0$ (empty lattice), (b) $\phi_0 = 0.4\pi$. In both cases, $a_0^0 = 1$ and all other elements are initially set to zero.

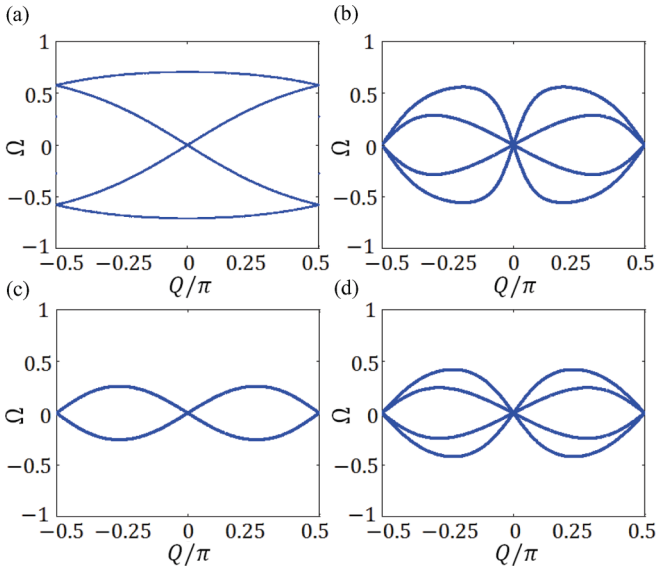

FIG. 7. (Color online) Beam tangent angle (Ω) for several cases: (a) empty lattice (note that in this case the curve is folded to the reduced Brillouin zone), (b) for a lattice in the presence of periodic phase potential with $\phi_0 = 0.2\pi$, (c) $\phi_0 = 0.5\pi$, and (d) $\phi_0 = 0.7\pi$.

can be obtained by expanding the propagation constant θ in a Taylor series around Q_0, that is,

$$\theta = \theta_0 + \frac{d\theta}{dQ}_{|_{Q_0}} (Q - Q_0) + \frac{d^2\theta}{dQ^2}_{|_{Q_0}} (Q - Q_0). \tag{8}$$

As in continuous lattices, the tangent of the beam angle (or "group velocity") is associated with the term

$$\Omega = \frac{d\theta}{dQ}_{|_{Q_0}}. \tag{9}$$

Using the dispersion given by Eq. (4), this group speed can then be written as

$$\frac{d\theta}{dQ} = \frac{1}{4} \frac{\sin(2Q)}{[\sin(2\theta) - \cos(\phi_0)\sin(\theta)]}, \tag{10}$$

where in this relation θ could be replaced from the dispersion relation of Eq. (5) to obtain the right-hand side as a function of Q and the band under consideration. Using similar arguments, the discrete diffraction factor can be obtained from

$$D = \frac{d^2\theta}{dQ^2}_{|_{Q_0}}. \tag{11}$$

Figure 7 depicts the beam angle Ω for several lattices with different amplitudes of the phase potential, ϕ_0. According to this figure, in an empty lattice ($\phi_0 = 0$), this beam angle is zero at the center ($Q = 0$) and it is maximum at $Q = \theta = 0$ in the folded Brillouin-zone scheme, where to first order the dispersion relation dictates that $Q = \pm\sqrt{2}\theta$. Hence, as previously indicated, the maximum slope expected in this configuration is $\Omega_{\max} = \pm 1/\sqrt{2}$. On the other hand, for a lattice having a periodic phase potential, each band exhibits a zero group velocity at the center and at the edges ($Q = \pm\pi/2$) of the zone, while the maximum happens somewhere in between. For the special case of $\phi_0 = \pi/2$, the bands are translated in θ and hence in groups of two have identical group velocity curves, and, as shown in Fig. 7(c), they lie on top of each other.

To demonstrate some of these transport effects, let us consider, for example, the evolution of a Gaussian wave packet having the following initial profile:

$$a_n^0 = e^{-(n/\Delta)^2} e^{iQ_0 n}, \tag{12}$$

where 2Δ represents the Gaussian beamwidth and Q_0 designates the initial tilt in its phase front or central Bloch momentum. In this case, the same input profile is assumed for b_n^0 in order to symmetrize the dynamics. Figure 8 shows the propagation dynamics of this Gaussian beam in this mesh lattice. Here the lattice involves a periodic phase potential with $Q_0 = 0.2\pi$. The Gaussian beam width 2Δ is large enough to avoid the diffraction effects and, in addition, its tilt is $Q_0 = 0.25\pi$. According to this figure, four independent beams (of the same width) result from this initial excitation, each emanating from a corresponding band and propagating in different directions. To elucidate these results, the band structure is also plotted in this same Fig. 8(c), where the arrows perpendicular to the bands indicate the propagation direction of each of these four beams.

Finally, in order to investigate diffraction effects in passive mesh systems, we consider the propagation properties of a relatively narrow Gaussian wave packet. Figure 9 depicts the propagation dynamics of a Gaussian beam with a width of $2\Delta = 8$ in a lattice with $\phi_0 = 0.5\pi$. The figures compare the beam propagation for two different values of Q_0, 0 and 0.25π. According to this figure, when $Q_0 = 0$, the beam has a very low transverse velocity and experiences a considerable degree of diffraction. As shown in the other panels, when the beam is launched at the dispersion-free point of the band ($Q_0 = 0.25\pi$), where $D = 0$ and the transverse group velocity is maximum, the diffraction effects are negligible.

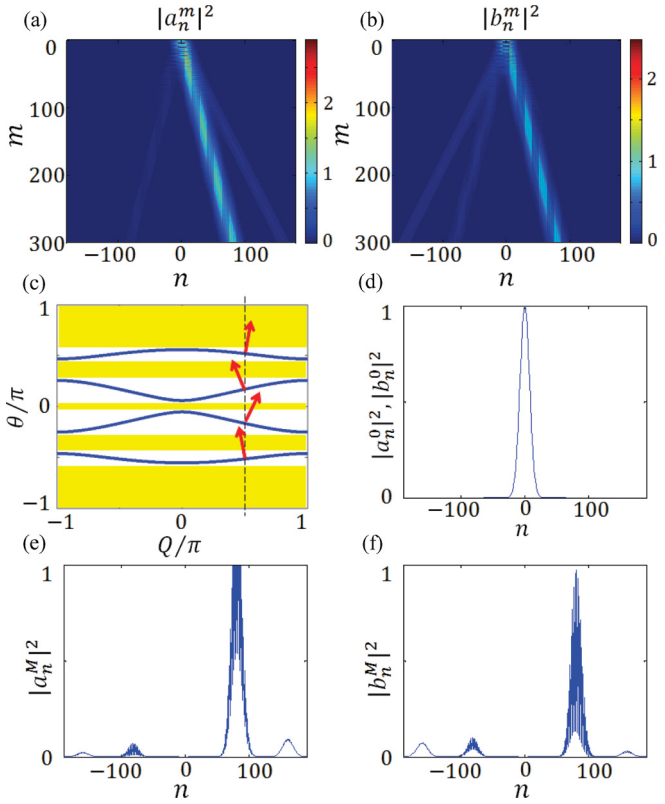

FIG. 8. (Color online) Gaussian wave packet propagating in a mesh lattice. The beam has a width of $2\Delta = 30$ and an initial phase tilt of $Q_0 = 0.25\pi$. The lattice has a phase potential of $\phi_0 = 0.2\pi$. (a) Intensity $|a_n^m|^2$, (b) intensity of $|b_n^m|^2$, (c) band structure of the lattice with the dashed line crossing the band at four points at $Q_0 = 0.25\pi$ and where the arrows show the propagation direction of the four resulting beams, (d) intensity profile of the initial Gaussian beam, (e) $|a_n^M|^2$ intensity profile of a_n^m at the last discrete longitudinal step (here $M = 300$), and (f) $|b_n^M|^2$.

According to Fig. 4, this selection of ϕ_0 leads to four bands. Figure 9(a) depicts Gaussian beam spreading at $Q_0 = 0$ and, at the same time, interference effects resulting from the excitation of multiple bands. On the other hand, for $Q_0 = 0.25\pi$, two Gaussian beams symmetrically emerge with two different propagation speeds. Yet, the interference pattern in each of the two branches demonstrates that all four bands are actually in play in these dynamics. Notice, however, that at this point little beam spreading occurs, since for these parameters $D = 0$.

V. $\mathcal{PT}$-SYMMETRIC BUILDING BLOCK

Before exploring a large-scale $\mathcal{PT}$-symmetric mesh lattice, it is worth analyzing the elemental building block involved in such a network. Figure 10(a) shows a $\mathcal{PT}$-symmetric coupler where the gain and loss is uniformly distributed along the two arms, which is a structure similar to that considered in previous experimental studies [22,23]. Figure 10(b), on the other hand, depicts a passive coupler where the gain and loss mechanisms are separately inserted in the two arms only. Here we show that this type of $\mathcal{PT}$-symmetric coupler displays exactly the same behavior and characteristics as a standard $\mathcal{PT}$-coupler arrangement considered before.

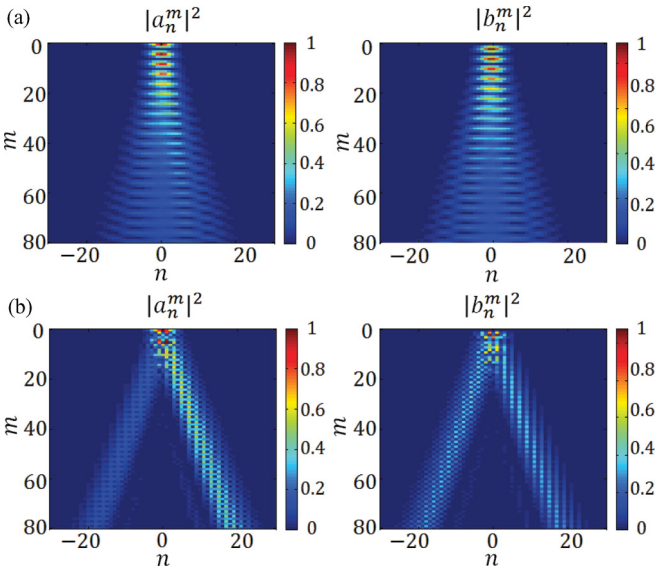

FIG. 9. (Color online) Diffraction properties of a Gaussian beam in a mesh lattice with $\phi_0 = 0.5\pi$. The Gaussian beam has a width of $2\Delta = 8$, while the initial phase tilt is (a) $Q_0 = 0$ and (b) $Q_0 = 0.25\pi$.

In Fig. 10(b), we assume a 50:50 passive directional coupler connected to two arms, with one providing amplification (red) while the other provides an equal amount of loss (blue). We assume that each arm delivers an amplification or attenuation of $e^{\pm\gamma/2}$ right before and after the coupler. Hence, the modal amplitudes a' and b' at the output of this system are related to those at the input ports, a and b, in the following way:

$$\begin{pmatrix} a' \\ b' \end{pmatrix} = \begin{pmatrix} e^{+\gamma/2} & 0 \\ 0 & e^{-\gamma/2} \end{pmatrix} \frac{1}{\sqrt{2}} \begin{pmatrix} 1 & i \\ i & 1 \end{pmatrix} \begin{pmatrix} e^{+\gamma/2} & 0 \\ 0 & e^{-\gamma/2} \end{pmatrix} \begin{pmatrix} a \\ b \end{pmatrix}, \tag{13}$$

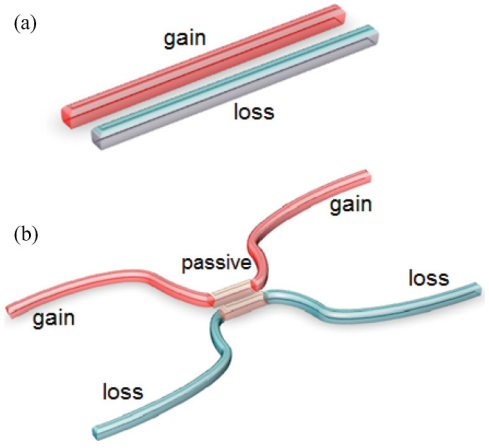

FIG. 10. (Color online) A distributed $\mathcal{PT}$-symmetric coupler and a $\mathcal{PT}$-synthetic coupler. (a) The $\mathcal{PT}$ coupler is composed of two similar dielectric waveguides coupled to each other, with one experiencing gain (red), while the other experiences an equal amount of loss (blue). (b) A $\mathcal{PT}$-synthetic coupler is composed of a passive coupler, while the gain and loss waveguides are separately used in the arms.

in which case

$$\begin{pmatrix} a' \\ b' \end{pmatrix} = \frac{1}{\sqrt{2}} \begin{pmatrix} e^{+\gamma} & i \\ i & e^{-\gamma} \end{pmatrix} \begin{pmatrix} a \\ b \end{pmatrix}, \tag{14}$$

where a and b represent optical amplitudes in the gain and loss channels, respectively. The two supermodes and their respective eigenvalues of this system can be readily found. Depending on the amount of gain-loss in the system, two regimes can be distinguished: if $\gamma < \cosh^{-1}(\sqrt{2})$, then this $\mathcal{PT}$ system is operating below the $\mathcal{PT}$-symmetry breaking threshold and its supermodes are given by

$$\begin{pmatrix} a_0 \\ b_0 \end{pmatrix} = \begin{pmatrix} 1 \\ \pm e^{\pm i\eta} \end{pmatrix} e^{\pm i\omega}, \tag{15}$$

where $\cos(\omega) = \frac{1}{\sqrt{2}}\cosh(\gamma)$ and $\sin(\omega) = \frac{1}{\sqrt{2}}\cos(\eta)$. Thus, for $\gamma < \cosh^{-1}(\sqrt{2})$, the two modes repeat themselves after passing through this discrete system, except from a trivial phase shift of $\pm\omega$. On the other hand, if $\gamma > \cosh^{-1}(\sqrt{2})$, then the system operates above the $\mathcal{PT}$-symmetry breaking threshold and

$$\begin{pmatrix} a_0 \\ b_0 \end{pmatrix} = \begin{pmatrix} 1 \\ i e^{\mp\eta} \end{pmatrix} e^{\pm\omega}, \tag{16}$$

where $\cosh(\omega) = \frac{1}{\sqrt{2}}\cosh(\gamma)$ and $\sinh(\omega) = \frac{1}{\sqrt{2}}\sinh(\eta)$. Interestingly, this same behavior is displayed by a standard $\mathcal{PT}$-symmetric coupler where the gain and loss is continuously distributed. Finally, at exactly the $\mathcal{PT}$-symmetry breaking threshold $\gamma = \cosh^{-1}(\sqrt{2})$, the two supermodes collapse to one and thus

$$\begin{pmatrix} a_0 \\ b_0 \end{pmatrix} = \begin{pmatrix} 1 \\ i \end{pmatrix}, \tag{17}$$

which clearly shows the existence of a phase difference of $\pi/2$ between the two waveguides.

It is worth noting that this arrangement has certain advantages over a standard distributed $\mathcal{PT}$-symmetric coupler. First of all, it is experimentally easier to achieve the delicate balance required for $\mathcal{PT}$ symmetry. In addition, the coupling and amplification or attenuation process take place in two separate steps, so there are no physical restrictions imposed by the Kramers-Kronig relations. As previously mentioned, these effects have so far hindered progress in implementing large-scale $\mathcal{PT}$-symmetric networks, since they limit the possibility of achieving the required values for gain-loss and refractive index at the same time.

VI. $\mathcal{PT}$-SYNTHETIC MESH NETWORKS

Figure 11(a) shows a $\mathcal{PT}$-symmetric mesh lattice made of $\mathcal{PT}$-synthetic couplers, identical to that of Fig. 10(b). In addition, phase elements are inserted in this same lattice [shown by circles in Fig. 11(a)] in order to provide the needed real part in the potential function. In Fig. 11(b), the distributions of phase modulation and that of gain-loss are plotted as a function of the discrete position n, clearly satisfying the requirement for $\mathcal{PT}$ symmetry, i.e., an even distribution for the phase and an odd distribution for the gain-loss profile in n. In fact, a comparison with continuous systems suggests that the phase and gain-loss in discrete elements play the role of the real

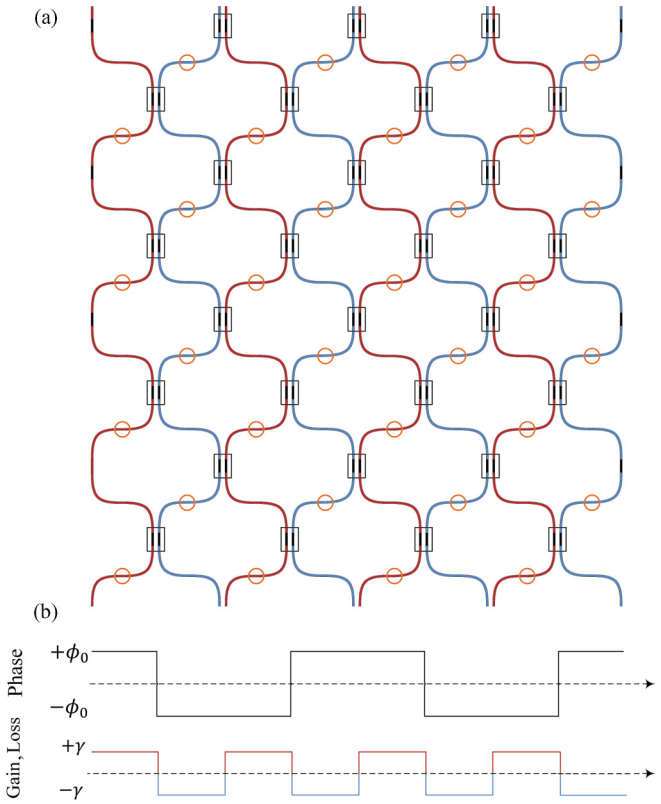

FIG. 11. (Color online) (a) A $\mathcal{PT}$-synthetic mesh lattice; (b) transverse distribution of the phase potential (symmetric) and gain and loss (antisymmetric).

and imaginary parts in the refractive index, respectively. By considering an amplification-attenuation factor of $e^{\pm\gamma/2}$ in each waveguide section between two subsequent couplers, one can show that light propagation in this $\mathcal{PT}$-synthetic mesh network is governed by the following discrete evolution equations:

$$a_n^{m+1} = \frac{e^{i\phi_n}}{2}\left[e^{-\gamma}\left(a_n^m + ib_n^m\right) + e^{-i\phi_n}\left(-a_{n-1}^m + ib_{n-1}^m\right)\right], \tag{18a}$$

$$b_n^{m+1} = \frac{e^{i\phi_n}}{2}\left[e^{+\gamma}\left(b_n^m + ia_n^m\right) + e^{i\phi_{n+1}}\left(-b_{n+1}^m + ia_{n+1}^m\right)\right]. \tag{18b}$$

To understand the behavior of this system, the band structure should be first determined. By adopting the same ansatz of Eq. (3), one can derive the following dispersion relation for this $\mathcal{PT}$ lattice:

$$\cos(2Q) = 8\cos^2(\theta) - 8\cosh(\gamma)\cos(\phi_0)\cos(\theta) + 4\cos^2(\phi_0) - 4 + \cosh(2\gamma). \tag{19}$$

Figure 12 shows the band structure of this system for several different values of the phase potential amplitude ϕ_0 and gain-loss coefficients γ. In each case, the real parts of the propagation constant (θ) are plotted in blue, while the imaginary parts are shown in red.

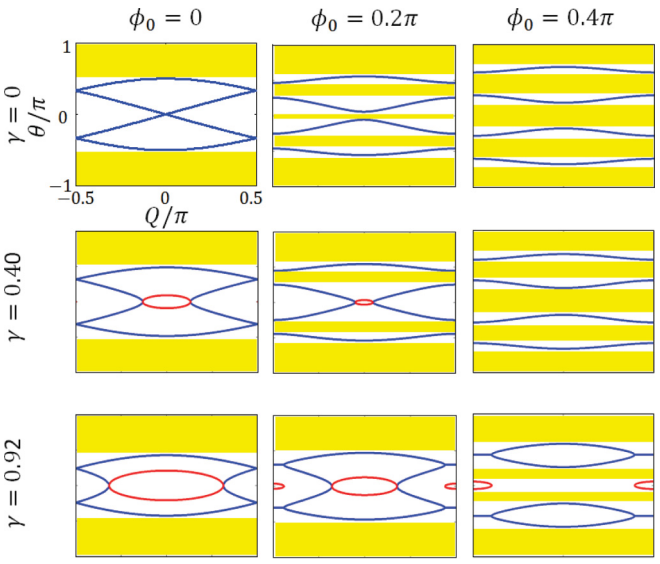

FIG. 12. (Color online) Band structure of $\mathcal{PT}$-synthetic mesh lattice for several values of ϕ_0 and γ. In these plots, the real part of propagation constant θ is indicated in blue, while the imaginary part is indicated in red.

As illustrated in this figure, the presence of a symmetric phase potential in this system tends to pull apart the bands thus creating a band gap, while the antisymmetric gain-loss tends instead to close the gap. The system is said to be operating below the $\mathcal{PT}$-symmetry-breaking threshold as long as the eigenvalues associated with all bands are real. However, at a critical amount of gain-loss, the bands merge at the so-called exceptional points, and for even higher gain-loss values, sections with conjugate imaginary eigenvalues appear in the bands.

In what follows, we consider the case where ϕ_0 is fixed and discuss how the band structure will change by gradually increasing the gain-loss coefficient γ. Analysis shows that for a given value of ϕ_0, the first band merging occurs at two different positions; if $0 < \phi_0 < \pi/4$, then the bands merge at $Q = \theta = 0$ and the second band gap remains open until it reaches a critical value of gain-loss coefficient γ. For even higher gain-loss values, the system finds itself in the broken phase regime. For $\pi/4 < \phi_0 < \pi/2$, on the other hand, all bands are open until a critical point. Exactly at this threshold, the band gap at the edges of the Brillouin zone at $Q = \pm\pi/2$ closes, while the first band gap remains open until it reaches another critical point where it eventually evaporates. Based on these observations, analytical results for the symmetry-breaking point can be obtained. We first consider the case where $0 < \phi_0 < \pi/4$. In this case, as γ increases, we expect that for a fixed ϕ_0, the symmetry breaking will occur at $Q = \theta = 0$. Therefore, Eq. (19) can be rewritten as

$$\cosh^2(\gamma) - 4\cos(\phi_0)\cosh(\gamma) + 2\cos^2(\phi_0) + 1 = 0. \quad (20)$$

From here, one can easily show that this critical γ is given by

$$\gamma = \cosh^{-1}[2\cos(\phi_0) - \sqrt{\cos(2\phi_0)}]. \quad (21)$$

This relation dictates the merging condition for the first two bands and is only valid for $0 < \phi_0 < \pi/4$, which is consistent with our previous observations. To find the corresponding

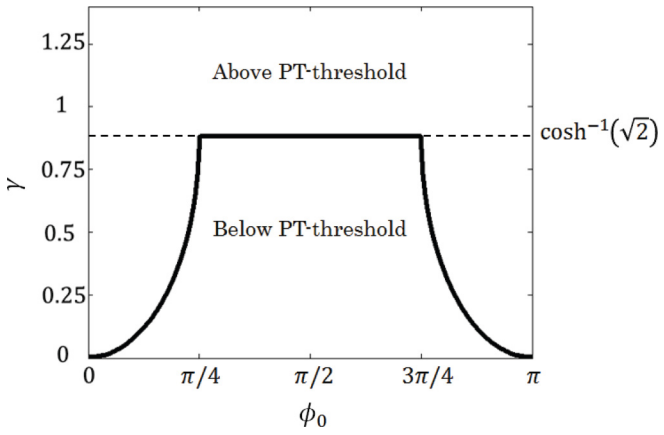

FIG. 13. $\mathcal{PT}$-symmetry-breaking threshold curve in a two-dimensional parameter space of ϕ_0 and γ. The region below the curve corresponds to the exact $\mathcal{PT}$ phase, while the region above the curve designates the domain where $\mathcal{PT}$ symmetry is broken.

relation for the band merging occurring at the edges, in Eq. (19) we set $Q = \pi/2$, which in turn leads to a second-order algebraic equation in $\cos(\theta)$. Since we expect that the two eigenvalues will collapse into one (exceptional point), one may use this degeneracy condition in Eq. (19) at $Q = \pi/2$. After setting the discriminant of the quadratic equation to zero, one finds that

$$\gamma = \cosh^{-1}(\sqrt{2}) \approx 0.8814. \quad (22)$$

This last relation provides the $\mathcal{PT}$ threshold for band merging at the edges of the Brillouin zone and is independent of ϕ_0. Interestingly, this same value $\gamma = \cosh^{-1}(\sqrt{2})$ coincides with the critical $\mathcal{PT}$ threshold of the basic unit involved in this lattice, as found in Sec. V.

Figure 13 depicts the $\mathcal{PT}$-symmetry-breaking threshold in the parameter space of ϕ_0 and γ. The area below the curve corresponds to the case where the system operates in the exact $\mathcal{PT}$ phase, where all of the eigenvalues are real. On the curve, symmetry breaking occurs and, above this line, the spectrum is, in general, complex. The top flat line of this curve corresponds to the critical value of 0.8814, while the part between $0 < \phi_0 < \pi/4$ can be obtained from Eq. (21). The other segment symmetrically follows.

To dynamically explore the symmetry-breaking threshold, the impulse response of our system is studied. Since the impulse is expected to excite the entire band of this mesh lattice, one should expect that an exponential growth in the total energy of the system should be observed once the $\mathcal{PT}$ symmetry is broken.

Figure 14 shows the impulse response ($a_n^0 = 1$, while all other elements are initially zero) of a $\mathcal{PT}$-symmetric mesh lattice for several different values of gain-loss γ when $\phi_0 = 0.2\pi$. This range covers the passive scenario, or the case where the system operates below, at, and above the $\mathcal{PT}$-symmetry-breaking threshold. The total energy in the system, $E_m = \sum_n |a_n^m|^2 + |b_n^m|^2$, is also plotted in each case at each discrete step of propagation, m, in Fig. 14. While for the passive system ($\gamma = 0$) the total energy remains constant during propagation, for a $\mathcal{PT}$-symmetric lattice used below its threshold the total energy tends to oscillate during

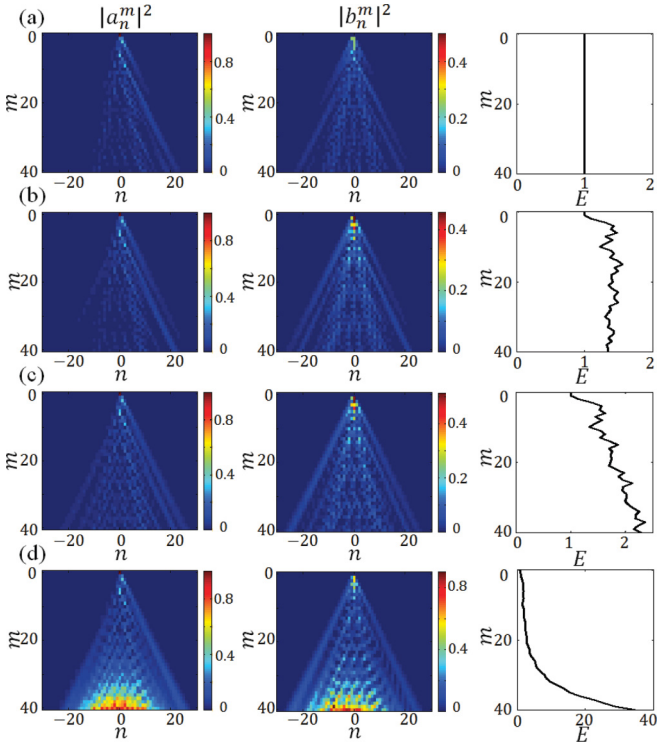

FIG. 14. (Color online) Impulse response of the $\mathcal{PT}$-symmetric lattice with a periodic phase potential of $\phi_0 = 0.2\pi$, while several different amounts of gain-loss are considered: (a) $\gamma = 0$ (the passive lattice), (b) $\gamma = 0.3$ (below threshold), (c) $\gamma = 0.35$ (at threshold), and (d) $\gamma = 0.4$ (above threshold).

propagation—but always remains below a certain bound. Note that such power oscillations were previously encountered in other $\mathcal{PT}$-symmetric periodic structures [18]. At exactly the $\mathcal{PT}$ threshold, a linear growth in energy is observed; see Fig. 14(c). Finally, above threshold, an exponential growth in energy is observed, as expected from a system involving complex eigenvalues; see Fig. 14(d).

To further explore the behavior of this $\mathcal{PT}$-synthetic mesh lattice, we use at the input a Gaussian wave packet, as in Eq. (12). Indeed, by exciting this system with a wide input beam (that has a narrow spectrum), one can selectively excite different sections of the band structure. We now consider a $\mathcal{PT}$-symmetric mesh lattice with a periodic phase potential of amplitude $\phi_0 = 0.2\pi$ and a gain-loss factor of $\gamma = 0.4$. The band structure corresponding to this structure is plotted in Fig. 12.

Figure 15 depicts the propagation of a Gaussian wave packet in this lattice, when launched with a Bloch momentum Q_0. Three different values for Q_0 have been selected for this example: $Q_0 = 0$, 0.25π, and 0.5π. According to Fig. 15, while for the first case an exponential energy growth is observed, for the other two cases energy remains essentially bounded. These results reveal that even above the $\mathcal{PT}$-symmetry-breaking threshold, nongrowing or decaying modes can be excited in such systems. This all depends on which section of the band structure is excited by the initial conditions.

Compared to a passive mesh lattice, the band structure of its $\mathcal{PT}$-symmetric counterpart reveals another interesting property. As previously discussed, the maximum beam transport angle ($\Omega_{\max}$) in an empty lattice is $1/\sqrt{2}$, and even in the presence of a periodic phase potential, this angle is always less than this maximum transverse velocity. However, according to Fig. 12, when approaching the exceptional points from the real section (blue part) of the band, its slope tends to considerably increase and eventually approaches infinity around the exceptional points.

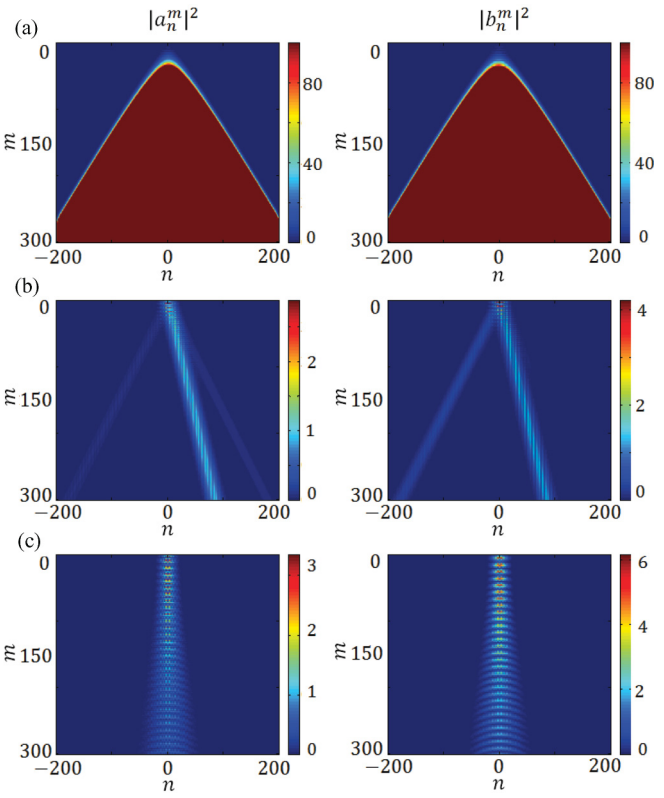

FIG. 15. (Color online) Gaussian beam propagation in a $\mathcal{PT}$-symmetric lattice operating in the broken $\mathcal{PT}$ phase regime. The lattice has a periodic phase potential of amplitude $\phi_0 = 0.2\pi$ and a gain-loss factor of $\gamma = 0.4$. The Gaussian beam has a width of $2\Delta = 30$ and is launched with three different values of initial phase tilt: $Q_0 =$ (a) 0, (b) 0.25π, and (c) 0.5π. In (a), the intensities are only shown up to a level of 100.

Figure 16 compares the propagation of a Gaussian beam in a passive and a $\mathcal{PT}$-symmetric mesh lattice operating above threshold. Both lattices are excited with the same Gaussian beam having a Bloch momentum Q_0, which is chosen to be close to the exceptional point of the $\mathcal{PT}$-symmetric lattice. Close to this exceptional point, the slope of the band structure tends to infinity and, therefore, the associated group velocity can become almost arbitrarily high for any narrow-bandwidth wave packet. While the maximum beam angle in the passive empty lattice is ~0.7 (which is close to the maximum), for the $\mathcal{PT}$-symmetric lattice this angle is approximately 1.04, which is certainly above the maximum limit of the passive lattice. This effect has, in fact, a counterpart in continuous media. As previously shown, in the presence of a gain medium [54,55] and in $\mathcal{PT}$-symmetric and gain-loss gratings and lattices [38, 56,57] used close to the exceptional points, the group velocity of light can be superluminal. It should be noted, however, that none of these effects violates causality since noncausal

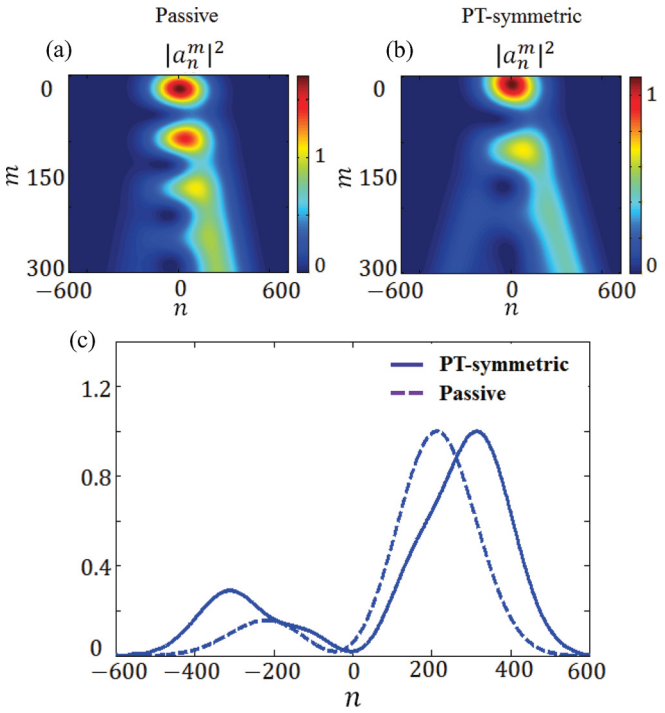

FIG. 16. (Color online) A broad Gaussian beam propagating in a passive and a $\mathcal{PT}$-symmetric lattice: (a) evolution of the Gaussian beam in a passive empty lattice, (b) in a $\mathcal{PT}$-symmetric lattice, and (c) normalized intensity profiles of the beam at the last propagation step ($m = 300$) in both lattices. The parameters of the $\mathcal{PT}$ lattice are $\gamma = 0.039$ and $\phi_0 = 0$. The Gaussian beam has a beam width of $2\Delta = 400$ and an initial phase front tilt of $Q_0 = 0.9817\pi$.

wave forms are used for excitation. Indeed, this superluminal propagation of the intensity peak is enabled by a gain-assisted growth of the distribution's tails.

Finally, we investigate the concept of unidirectional invisibility in a $\mathcal{PT}$-symmetric mesh lattice. As recently predicted [35,36], $\mathcal{PT}$-symmetric periodic structures such as gratings can exhibit surprising behavior such as unidirectional invisibility and intriguing reflection characteristics. More specifically, light propagating in such a system can experience reduced or enhanced reflections depending on the direction of propagation. Even more remarkable is what happens right at $\mathcal{PT}$ threshold: in this case, light waves entering this arrangement from one side do not experience any reflection and can fully traverse the grating with unity transmission. Given that this occurs without acquiring any phase imprint from this $\mathcal{PT}$ system, the periodic structure is essentially invisible. Similar effects also occur in $\mathcal{PT}$-symmetric mesh lattices. This can be demonstrated in a system where one lattice is embedded in another lattice. This is achieved using, for example, the following phase modulation potential:

$$\phi_n = \begin{cases} 0, & |n| > n_0, \\ +\phi_0, & |n| < n_0, \ n = \text{even}, \\ -\phi_0, & |n| < n_0, \ n = \text{odd}, \end{cases} \tag{23}$$

where $2n_0$ is the width of this $\mathcal{PT}$ grating lattice. In this same way, the antisymmetric gain-loss profile is also imposed only in the grating region $|n| < n_0$.

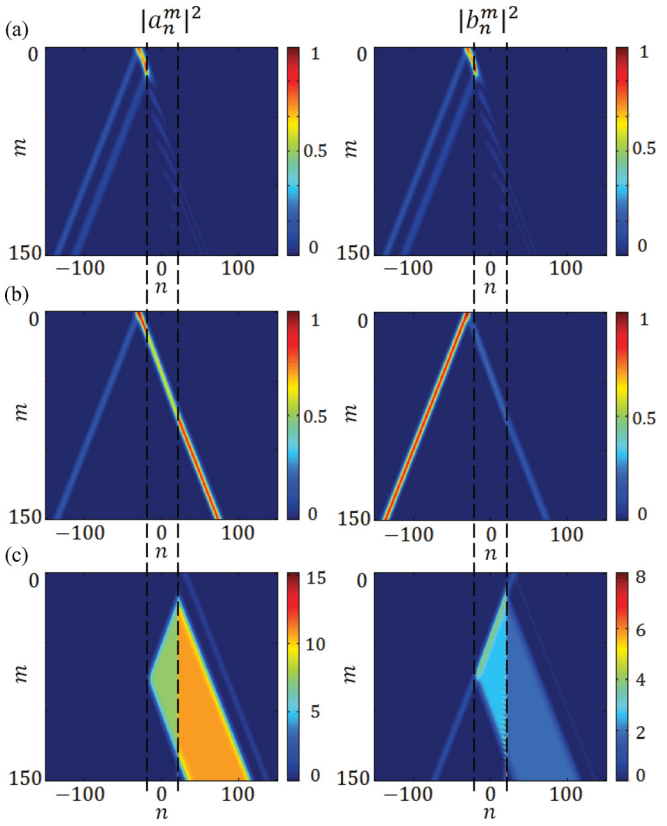

FIG. 17. (Color online) Unidirectional scattering of a Gaussian beam from a $\mathcal{PT}$-symmetric grating. A $\mathcal{PT}$-symmetric grating having 40 layers with a phase potential of $\phi_0 = 0.2\pi$ and a gain-loss of $\gamma = 0.3507$ (corresponding to $\mathcal{PT}$ threshold) is established in the middle of an empty lattice. The dashed line shows the grating region. (a) Scattering from the passive grating, (b) left-side scattering from this $\mathcal{PT}$-symmetric grating, and (c) right-side scattering from this same grating.

To investigate this latter process, a $\mathcal{PT}$-symmetric lattice having $2n_0 = 40$ layers is embedded inside an empty lattice. The empty lattice is excited with a Gaussian beam [as in Eq. (12)] with an initial phase tilt of $Q_0 = \pi$. The scattering of the beam from the left and right side of this $\mathcal{PT}$-symmetry grating is depicted in Fig. 17.

Figure 17 shows the scattering of Gaussian wave packet from this grating when $2n_0 = 40$, $\phi_0 = 0.2\pi$, and $\gamma = 0.3507$. The extent of this grating is shown by the dashed lines. Figure 17(a) shows how the Gaussian beam is scattered or transmitted by this grating when $\gamma = 0$. The effects of reflection and reduced transmission are evident in this figure. In Fig. 17(b), we show these same dynamics for $\gamma = 0.3507$ and for when the Gaussian excites the grating from the left. Both the a_n^m and b_n^m channels are excited during this process. In this case, no reflections occur when the grating is used close to the exceptional point. Essentially, in this regime, the grating leaves no mark on the beam itself and hence is practically invisible. Note that the associated splinter beams in this figure do not represent reflections—they simply emerge from the two different bands associated with the empty lattice. On the other hand, Fig. 17(c) shows what will happen when the Gaussian beam excites the right side of this same $\mathcal{PT}$-symmetric lattice

grating. In this latter case, pronounced reflections occur (even exceeding unity) and the grating ceases to be invisible to light.

VII. CONCLUSIONS

In this work, we have studied the properties of a class of periodic structures both in the passive as well as in the $\mathcal{PT}$-symmetric regime. These optical mesh lattices are, in essence, waveguide arrays that are discretely and periodically coupled to each other along the propagation direction. In addition, phase elements can also be used in appropriate positions to control the phases, while amplifiers and attenuators can be employed to realize the antisymmetric imaginary part of the $\mathcal{PT}$ potential. What makes these optical lattices different from previously known waveguide array versions is the presence of discreetness in both the transverse and longitudinal directions. The band structure of these systems has been systematically analyzed and an analytic expression was obtained for their dispersion relation. We have shown that the band structure is periodic in both the propagation constant and transverse Bloch momentum, while the Brillouin zone of these lattices displays, in general, four bands. In addition, we found that the shape of the bands and band gaps can be effectively controlled using phase elements. Interestingly, through a proper phase modulation, the band structure can be arbitrarily shifted from the center. It should be noted that shifting the bands in standard optical waveguide array systems is not straightforward and typically requires the presence of external magnetic field effects. The impulse light dynamics as well as wave-packet excitations were numerically explored and related to the properties of the band structure. The elementary $\mathcal{PT}$ building block involved in these mesh arrangements was examined and its symmetry-breaking threshold was determined. As discussed, what could greatly facilitate the physical realization of such a large scale $\mathcal{PT}$-symmetric mesh lattice is the fact that couplings and amplification-attenuation can be independently controlled within the basic building block of this lattice. Band-merging effects in these lattices were investigated and the conditions for spontaneous $\mathcal{PT}$-symmetry breaking were explicitly obtained in terms of relevant parameters. The response of these systems under impulse and broad beam excitation was investigated in terms of their respective band structure. As was shown, light dynamics in the $\mathcal{PT}$-symmetric lattice exhibits certain peculiarities that are otherwise impossible in its passive counterpart. These include, for example, power oscillations and transitions from neutral to exponentially growing regimes. The possibility of superluminal transport along with unidirectional invisibility was also considered.

ACKNOWLEDGMENTS

This work has been partially supported by NSF Grant No. ECCS-1128520 and AFOSR Grant No. FA95501210148. It was also funded by DFG Forschergruppe 760, the Cluster of Excellence Engineering of Advanced Materials and School of Advanced Optical Technologies (SAOT).

[1] J. D. Joannopoulos, S. G. Johnson, J. N. Winn, and R. D. Meade, *Photonic Crystals: Molding the Flow of Light*, 2nd ed. (Princeton University Press, Princeton, 2008).
[2] E. Yablonovitch, Phys. Rev. Lett. **58**, 2059 (1987).
[3] S. John, Phys. Rev. Lett. **58**, 2486 (1987).
[4] K. O. Hill, Y. Fujii, D. C. Johnson, and B. S. Kawasaki, Appl. Phys. Lett. **32**, 647 (1978).
[5] P. Russell, Science **299**, 358 (2003).
[6] D. N. Christodoulides, F. Lederer, and Y. Silberberg, Nature (London) **424**, 817 (2003); D. N. Christodoulides and R. I. Joseph, Opt. Lett. **13**, 794 (1988).
[7] H. S. Eisenberg, Y. Silberberg, R. Morandotti, A. R. Boyd, and J. S. Aitchison, Phys. Rev. Lett. **81**, 3383 (1998); R. Morandotti, U. Peschel, J. S. Aitchison, H. S. Eisenberg, and Y. Silberberg, *ibid.* **83**, 2726 (1999); D. Mandelik, R. Morandotti, J. S. Aitchison, and Y. Silberberg, *ibid.* **92**, 093904 (2004).
[8] J. W. Fleischer, M. Segev, N. K. Efremidis, and D. N. Christodoulides, Nature (London) **422**, 147 (2002); O. Cohen, G. Bartal, H. Buljan, T. Carmon, J. W. Fleischer, M. Segev, and D. N. Christodoulides, *ibid.* **433**, 500 (2004).
[9] R. Morandotti, U. Peschel, J. S. Aitchison, H. S. Eisenberg, and Y. Silberberg, Phys. Rev. Lett. **83**, 4756 (1999).
[10] T. Pertsch, P. Dannberg, W. Elflein, A. Bräuer, and F. Lederer, Phys. Rev. Lett. **83**, 4752 (1999).
[11] H. Trompeter, W. Krolikowski, D. N. Neshev, A. S. Desyatnikov, A. A. Sukhorukov, Y. S. Kivshar, T. Pertsch, U. Peschel, and F. Lederer, Phys. Rev. Lett. **96**, 053903 (2006); H. Trompeter, T. Pertsch, F. Lederer, D. Michaelis, U. Streppel, A. Bräuer, and U. Peschel, *ibid.* **96**, 023901 (2006).
[12] T. Schwartz, G. Bartal, S. Fishman, and M. Segev, Nature (London) **446**, 52 (2006); Y. Lahini, A. Avidan, F. Pozzi, M. Sorel, R. Morandotti, D. N. Christodoulides, and Y. Silberberg, Phys. Rev. Lett. **100**, 013906 (2008).
[13] K. Shandarova, C. E. Rüter, D. Kip, K. G. Makris, D. N. Christodoulides, O. Peleg, and M. Segev, Phys. Rev. Lett. **102**, 123905 (2009).
[14] A. Szameit, I. L. Garanovich, M. Heinrich, A. A. Sukhorukov, F. Dreisow, T. Pertsch, S. Nolte, A. Tünnermann, and Y. S. Kivshar, Nature Phys. **5**, 271 (2009).
[15] K. Staliunas and C. Masoller, Opt. Express **14**, 10669 (2006); S. Longhi and K. Staliunas, Opt. Commun. **281**, 4343 (2008).
[16] G. Lenz, R. Parker, M. Wanke, and C. de Sterke, Opt. Commun. **218**, 87–92 (2003); S. Longhi, Opt. Lett. **30**, 2137 (2005).
[17] R. El-Ganainy, K. Makris, D. Christodoulides, and Z. Musslimani, Opt. Lett. **32**, 2632 (2007).
[18] K. G. Makris, R. El-Ganainy, D. N. Christodoulides, and Z. H. Musslimani, Phys. Rev. Lett. **100**, 103904 (2008).
[19] Z. H. Musslimani, K. G. Makris, R. El-Ganainy, and D. N. Christodoulides, Phys. Rev. Lett. **100**, 030402 (2008).
[20] C. M. Bender and S. Boettcher, Phys. Rev. Lett. **80**, 5243 (1998); C. M. Bender, Rep. Prog. Phys. **70**, 947 (2007); C. M. Bender, D. C. Brody, and H. F. Jones, Phys. Rev. Lett. **89**, 270401 (2002).

[21] G. Lévai and M. Znojil, J. Phys. A: Math. Gen. **33**, 7165 (2000); Z. Ahmed, Phys. Lett. A **282**, 343 (2001); Z. Ahmed, C. M. Bender, and M. V. Berry, J. Phys. A: Math. Gen. **38**, L627 (2005).
[22] A. Guo, G. J. Salamo, D. Duchesne, R. Morandotti, M. Volatier-Ravat, V. Aimez, G. A. Siviloglou, and D. N. Christodoulides, Phys. Rev. Lett. **103**, 093902 (2009).
[23] C. E. Ruter, K. G. Makris, R. El-Ganainy, D. N. Christodoulides, M. Segev, and D. Kip, Nature Phys. **6**, 192 (2010).
[24] K. G. Makris, R. El-Ganainy, D. N. Christodoulides, and Z. H. Musslimani, Phys. Rev. A **81**, 063807 (2010).
[25] S. Klaiman, U. Günther, and N. Moiseyev, Phys. Rev. Lett. **101**, 080402 (2008).
[26] M. C. Zheng, D. N. Christodoulides, R. Fleischmann, and T. Kottos, Phys. Rev. A **82**, 010103 (2010).
[27] A. A. Sukhorukov, Z. Xu, and Y. S. Kivshar, Phys. Rev. A **82**, 043818 (2010).
[28] A. E. Miroshnichenko, B. A. Malomed, and Y. S. Kivshar, Phys. Rev. A **84**, 012123 (2011).
[29] H. Ramezani, T. Kottos, R. El-Ganainy, and D. N. Christodoulides, Phys. Rev. A **82**, 043803 (2010).
[30] M.-A. Miri, P. LiKamWa, and D. N. Christodoulides, Opt. Lett. **37**, 764 (2012).
[31] S. Longhi, Phys. Rev. Lett. **103**, 123601 (2009).
[32] Y. D. Chong, L. Ge, and A. D. Stone, Phys. Rev. Lett. **106**, 093902 (2011).
[33] M. Liertzer, L. Ge, A. Cerjan, A. D. Stone, H. E. Türeci, and S. Rotter, Phys. Rev. Lett. **108**, 173901 (2012).
[34] S. Longhi, Phys. Rev. A **82**, 031801 (2010).
[35] Z. Lin, H. Ramezani, T. Eichelkraut, T. Kottos, H. Cao, and D. N. Christodoulides, Phys. Rev. Lett. **106**, 213901 (2011).
[36] M. Kulishov, J. Laniel, N. Belanger, J. Azana, and D. Plant, Opt. Express. **13**, 3068 (2005).
[37] H. Benisty, A. Degiron, A. Lupu, A. De Lustrac, S. Chenais, S. Forget, M. Besbes, G. Barbillon, A. Bruyant, S. Blaize, and G. Lerondel, Opt. Express. **19**, 18004 (2011).
[38] M.-A. Miri, A. B. Aceves, T. Kottos, V. Kovanis, and D. N. Christodoulides [Phys. Rev. A (to be published)].
[39] Y. N. Joglekar and J. L. Barnett, Phys. Rev. A **84**, 024103 (2011); H. Vemuri, V. Vavilala, T. Bhamidipati, and Y. N. Joglekar, *ibid.* **84**, 043826 (2011).
[40] E.-M. Graefe and H. F. Jones, Phys. Rev. A **84**, 013818 (2011).
[41] D. A. Zezyulin and V. V. Konotop, Phys. Rev. Lett. **108**, 213906 (2012).
[42] K. Staliunas, R. Herrero, and R. Vilaseca, Phys. Rev. A **80**, 013821 (2009).
[43] A. Regensburger, C. Bersch, B. Hinrichs, G. Onishchukov, A. Schreiber, C. Silberhorn, and U. Peschel, Phys. Rev. Lett. **107**, 233902 (2011).
[44] A. Schreiber, K. N. Cassemiro, V. Potocek, A. Gabris, P. J. Mosley, E. Andersson, I. Jex, and C. Silberhorn, Phys. Rev. Lett. **104**, 050502 (2010).
[45] A. Schreiber, K. N. Cassemiro, V. Potocek, A. Gabris, I. Jex, and C. Silberhorn, Phys. Rev. Lett. **106**, 180403 (2011).
[46] A. Schreiber, A. Gábris, P. P. Rohde, K. Laiho, M. tefanák, V. Potocek, C. Hamilton, I. Jex, and C. Silberhorn, Science **336**, 55 (2012).
[47] M. A. Broome, A. Fedrizzi, B. P. Lanyon, I. Kassal, A. Aspuru-Guzik, and A. G. White, Phys. Rev. Lett. **104**, 153602 (2010).
[48] D. Bouwmeester, I. Marzoli, G. P. Karman, W. Schleich, and J. P. Woerdman, Phys. Rev. A **61**, 013410 (1999).
[49] L. Sansoni, F. Sciarrino, G. Vallone, P. Mataloni, A. Crespi, R. Ramponi, and R. Osellame, Phys. Rev. Lett. **108**, 010502 (2012).
[50] A. Regensburger, C. Bersch, M.-A. Miri, G. Onishchukov, D. N. Christodoulides, and U. Peschel [Nature (London) (to be published)] .
[51] J. Kempe, Contemp. Phys. **44**, 307 (2003).
[52] P. L. Knight, E. Roldán, and J. E. Sipe, Phys. Rev. A **68**, 020301 (2003).
[53] A. Yariv and P. Yeh, *Photonics: Optical Electronics in Modern Communications* (Oxford University Press, New York, 2007).
[54] R. Y. Chiao, Phys. Rev. A **48**, R34 (1993).
[55] L. J. Wang, A. Kuzmich, and A. Dogariu, Nature (London) **406**, 277 (2000).
[56] M. Botey, R. Herrero, and K. Staliunas, Phys. Rev. A **82**, 013828 (2010).
[57] A. Szameit, M. C. Rechtsman, O. Bahat-Treidel, and M. Segev, Phys. Rev. A **84**, 021806 (2011).